Regulation of Cooling and Star Formation in Giant Elliptical Galaxies by Supermassive Black Holes

Farnoud Kazemzadeh

20131959

Physics 437B, University of Waterloo

April 16, 2008

Supervisor: Dr. Brian McNamara

fkazemza@sciborg.uwaterloo.ca

1. Abstract

Star formation and nuclear activity may be fueled by gas cooling and condensing out of the hot, X-ray coronae of giant elliptical galaxies. The rate of cooling, which is proportional to the X-ray luminosity of the hot corona, exceeds the star formation rate by large factors. Star formation may be suppressed by radio outbursts (AGN) driven by accretion onto the central, super massive black hole (BH). We test this by measuring star formation rates (SFR) in a sample of 18 gEs, and comparing them to the cooling rates and AGN power of the host galaxies. Higher star formation rates are observed in galaxies with higher X-ray luminous gEs. Star formation is suppressed in systems with a higher ratio of AGN heating to X-ray cooling (Fig. 4). Radio sources in gEs are radiatively inefficient and are dominated by mechanical energy by factors that can exceed one part in 10,000, making them efficient heaters of the surrounding gas. The growth of the black holes and the bulge of the galaxy obey Magorrian relation.

2. Introduction

Galaxies have formed $\sim$ 13 billion years ago are continuously growing. This growth is done in the form of star formation by repeated condensation from interstellar medium, and by mergers. The gas and dust mainly HI and HeI available in galaxies will cool (lower the temperature), condense and finally under gravitational instability collapse to form very dense regions. These regions would eventually turn on nuclear reactions and become stars (Evans 1999). For the purposes of this paper we will assume the most important step in star formation to be the cooling of the gas, which would lead to over dense regions and eventually to gravitational collapse and star formation.

Giant elliptical galaxies (gEs), or early type galaxies, are part of a cluster of galaxies and are home to $\sim 10^{11}$ - 10^{13} star most of which are old giant stars and star clusters. Normally, gEs have smooth and featureless light profiles. They are believed to have gone through a star formation phase, and have had finished the bulk of this process $\sim$ 6 - 10 billion years ago. So at this late stage of their lives, they should be merely free of gas and dust.

Typically the gas and dust are assumed to migrate to the central region of the gE. This is a manifestation of the fact that gas and dust can not be seen very well beyond the effective radius [half light radius (R_e)] of a gE (Knapp 1998). In order to observe the dust in gEs, (1) presence of a dust lane is necessary (NGC5128); (2) the gas/dust disk needs to be observed edge on and not face on; (3) the target needs to be observed in shorter wavelengths which are more affected by extinction (Knapp 1998). The presence and amount of gas is always inferred by the presence and the amount of dust because HI and HeI are not excited sufficiently to emit (Evans 1999). Albeit, HI concentrations are observed as H_α emission from the excitation of HI, this emission is only from the surface boundary of the gas concentration and does not represent the total amount of gas present in that region.

X-ray observations have shown that the space between galaxies in a galaxy cluster are

filled with a hot plasma of neutral Hydrogen. The concentration of this gas is higher in the halo of the galaxies. The sheer mass of these enormous galaxies creates a very deep potential well, and enables them to maintain this halo. The temperature of the halos are typically 10 - 100 million K (McNamara & Nulsen 2007). About 90% of the baryons in clusters reside in the plasma in the inter cluster medium (ICM) (Lin et al. 2003).

Exhaustive studies of central regions of nearby galaxies have demonstrated that there exists a dark massive object (black holes) $\sim 10^9 M_\odot$. Black holes (BH) are widely accepted to be the remnant of the past quasars (Soltan 1982). It is believed that black holes play a very important role in galaxy formation and evolution. Majority of the black holes in the local universe are currently quiescent, however there are a few that are active in a sense that there is material being accreted onto them. These galaxies are denoted as active galaxies. The central region of these active galaxies has a much higher luminosity than the starlight of the galaxy. The central region is also known as the active galactic nuclei (AGN). When material accretes onto the black hole a bipolar jet stream of energy and material is ejected from the black hole. This phenomenon is predominantly observed in radio wavelengths, as the result of synchrotron radiation of excited electrons.

A number of these powerful jet of relativistic particles and energy originated from the AGN is observed to have enough energy to be able to displace the halo gas and create holes in it. This was observed first in the 1980s in the Perseus cluster. Since then many more galaxies have been observed harboring similar structures (cavities). The cavities vary in size from diameters smaller that 1 kpc in M87 to diameters about 200 kpc in MS0735.6+7421 (McNamara & Nulsen 2007).

One of the most effective ways for the gas and dust in a cluster of galaxies to cool is thermal Bremsstrahlung emission in X-ray wavelengths (Sarazin 1988). Cooling flows are characterized by bright X-ray emission from dense gas in the ICM (Fabian 1994). Cooling

luminosity is commonly more that 10% of the clusters total luminosity and it varies from $\sim$ 10^{41} - 10^{45} ergs s^{-1} in most extreme cases of a centrally dominating galaxy (cD) (McNamara & Nulsen 2007). When the ICM gas cools below 10^4 K, it condenses onto the host galaxy. The hot gas surrounding then replaces the in-fallen gas, so this process creates a constant inward flow of gas and dust toward the center of the galaxy (Fabian 1994). The gas and dust will continue cooling while inside the galaxies potential well, and if there does not exist a mechanism to stop the cooling (heating) the gas will eventually condense into molecular clouds and in turn into stars. Luckily all the starlight in the galaxy is not sufficient to stop the cooling. However there are at least two mechanisms that are adequate in heating the gas in order to stop it from cooling and collapsing. The feedback from black holes and supernovae (Ia, II) are energetic enough to halt cooling of the gas. Supernovae are more effective in smaller galaxies but black holes can influence any size galaxy. For the purposes of this paper, feedback from supernovae are not deemed sufficient to halt cooling, therefore supernovae are not included.

In the paper the consequences of heating through AGN feedback and ICM cooling is used to investigate the star formation rate (SFR) in a sample of gEs which demonstrate a recent nuclear activity through observation of cavities. The radiative efficiency of the radio jets to create the cavities are investigated and the mass accretion rate onto the BH is calculated and correlated to the SFR to examine the Magorrian relation and the idea of galaxy growth. The preliminary results and conclusions are presented here. The results have not been corrected for Galactic extinction, evolutionary and K-correction. We assume $H_0 =$ 70 km $s^{-1}Mpc^{-1}$, $\Omega_\Lambda = 0.7$, and $\Omega_M = 0.3$ throughout.

3. The Sample

Our sample consists of 18 gEs in the local universe from redshifts z = 0.000047 to z = 0.034801, drawn from the works of Nulsen et al. 2006 for which GALEX data were available. Nulsen et al. have measured the X-ray luminosity (L_X) and the AGN power, or the energy needed to create the cavities in the halo normalized to the frequency of outbursts. The X-ray luminosity is measured by observing the galaxies in the X-ray wavelengths below 1 keV using Chandra X-ray Observatory. The data was then complemented by GALEX far and near UV, 2MASS near infrared (IR), and NVSS 20 cm (1400 MHz) radio observations. We note that our sample is biased to giant elliptical galaxies with observed cavity systems, hence our findings can not be generalized to all cooling flow galaxies. Table 1 (below) lists our sample and their intrinsic properties.

Table 1. Sample Properties

Target	z	Classification[b]	σ_c[a] (km s^{-1})	R_e[c] (kpc)
NGC315	0.016485	E	278.8±23.3	6.6778
NGC507	0.016458	SA	307±9.7	1.805
NGC777	0.016728	E1	324.1±10.6	5.902
NGC1316	0.00581	SAB	227.5±4.3	2.65
NGC1600	0.015614	E3	336±7.5	7.4[d]
NGC3077	0.000047	I0	···	0.3108
NGC3608	0.00418	E2	192.02±0.003	3.179
NGC4325	0.025714	E4	···	5.994
NGC4374	0.003536	E1	281.4±2.9	3.075
NGC4552	0.00134	E	252.4±3.4	0.4181
NGC5044	0.00902	E0	236.6±9.7	2.948
NGC5252	0.022975	S0	190±27	7.155
NGC5253	0.001358	Im Pec	···	0.924[d]
NGC5813	0.006578	E1-2	238.7±4.8	7.75[d]
NGC5846	0.005717	E0-1	236.8±4.4	2.489
NGC6269	0.0348108	E	229±10.9	2.63
NGC7626	0.01136	E Pec	275.1±5.2	2.896
UGC408	0.014657	SAB	···	0.9669

[a]The central velocity dispersion for the sample was retreived from Hyperleda database.

[b]The classification of the galaxies in our samples are retrieved from NASA Extragalactic Database (NED).

[c]The effective radii for the sample was derived from the Near-IR images using GALFIT by C. Peng.

[d]The R_e for these galaxies were adapted from the literature, NGC1600 - (Barbon et al. 1984), NGC5253 - (Marlowe et al. 1999), NGC5813 - (de Zeeuw et al. 2002)

4. Data and Data Analysis

4.1. Chandra X-ray Data

As mentioned before, the studied sample was drawn from the works of Nulsen who observed and processed the Chandra X-ray data. The presence of cavities in the sample was confirmed and their size and projected radii were determined. The cavities observed in the X-ray image allow for measurement of the energy output of the AGN assuming that the cavities are in pressure balance with the surrounding plasma. This allowed for the measurement of the BH energy output, and enabled the inference of the amount of mass accreted onto the BH per unit time under the assumption that the BH energy outburst created the cavities.

The energy needed to displace the volume of a sphere of the size of the cavity is evaluated using PV work, given by

$$E_{cav} = pV\frac{\gamma}{(\gamma - 1)} \tag{1}$$

where p is the pressure of the gas surrounding the cavity, V is the projected volume of the cavity, and γ is the ratio of the specific heat of the gas inside the cavity; for relativistic gas $\gamma = 4/3$. The mean power to create the cavity of a certain size would then be

$$P_{cav} = \frac{E_{cav}}{t} \tag{2}$$

where t is the average time between outbursts (Rafferty et al. 2006). Mass accreted onto the BH ($\dot{M}_{BH}$), in solar mass per year, was estimated assuming that the BH is only 10% efficient in converting the rest mass of the in-falling gas into outburst energy by using the relation derived by Rafferty et al. 2006

$$\dot{M}_{BH} = \frac{P_{cav}(1-\epsilon)}{(c^2\epsilon)}; \epsilon = 0.1 \tag{3}$$

From the same data the x-ray flux is determined within the cooling radius (R_{cool}). Cooling radius is a physical distance at which the surrounding plasma can cool and condense

onto the galaxy before the next outburst even happens $\sim$ 7.7 x 10^9 years (Bîrzan et al. 2004). The flux is then normalized to the outburst time scale and the x-ray luminosity is determined. The fact that the surrounding plasma is cooling signifies that there is gas and dust falling farther into the potential well of the host galaxy and eventually end up in the galaxy. And if the gas is allowed to cool then there should be some evidence of star formation. Also the fact that we seen such powerful AGN outburst tells us that not only there is gas and dust in the galaxy, hence fueling the BH, there is a heating mechanism that can stop the gas from cooling, in turn limit the stop formation and limit the amount of surrounding plasma cooling and condensing onto the galaxy. Table 2 (below) summarizes the deduced X-ray, cavity and ICM properties.

Table 2. Cavity and ICM Sample Properties from X-ray Observations

Target	P_{cav} (10^{40} erg s^{-1})	L_X [a] (10^{40} erg s^{-1})	R_{cool} (kpc)	$\dot{M}_{BH}$ [b] (10^{-5} $M_\odot$ yr^{-1})
NGC315	$352.42^{+262.41}_{-131.09}$	30.21	24.45	$56.7^{+42.22}_{-21.09}$
NGC507	$1285.99^{+437.72}_{-280.25}$	2086.9	113.59	$206.41^{+70.42}_{-45.09}$
NGC777	$274.65^{+204.23}_{-99.81}$	107.03	115.29	$44.19^{+32.86}_{-16.06}$
NGC1316	$60.6^{+22.64}_{-14.79}$	6.46	30.95	$10.39^{+3.64}_{-2.38}$
NGC1600	$102.21^{+107.29}_{-44.15}$	12.13	23.89	$16.44^{+17.26}_{-7.1}$
NGC3077	$15.12^{+17.85}_{-6.72}$	0.50	0.461	$2.43^{+2.87}_{-1.08}$
NGC3608	$3.37^{+1.74}_{-1.02}$	1.16	19.8	$2.43^{+0.28}_{-1.08}$
NGC4325	$1463.07^{+1412.45}_{-571}$	602.02	91.9	$235.39^{+227.24}_{-91.87}$
NGC4374	$237.36^{+261}_{-102.19}$	8.23	22.8	$38.19^{+41.99}_{-16.44}$
NGC4552	$26.76^{+8.74}_{-6.02}$	2.26	5.5	$4.31^{+1.41}_{-0.97}$
NGC5044	$281^{+132.18}_{-79.51}$	491.1	130.9	$45.21^{+21.27}_{-12.79}$
NGC5252	$37.15^{+18.41}_{-10.12}$	13.41	50.7	$5.98^{+2.96}_{-1.63}$
NGC5253	$0.34^{+0.38}_{-0.16}$	0.04	7.0	$0.06^{+0.06}_{-0.03}$
NGC5813	$240.91^{+148.45}_{-63.51}$	219.71	96.3	$38.76^{+23.88}_{-10.22}$
NGC5846	$51^{+32.9}_{-16.47}$	82.56	69.3	$8.2^{+5.29}_{-2.65}$
NGC6269	$126.33^{+84.01}_{-39.22}$	138.88	48.6	$20.32^{+13.52}_{-6.31}$
NGC7626	$28.63^{+13.5}_{-6.67}$	14.09	37.6	$4.61^{+2.17}_{-1.07}$
UGC408	$6764.28^{+3072.13}_{-2116.63}$	154.85	50.8	$1088.27^{+494.26}_{-340.21}$

[a]Bolometric X-ray luminosity measured within the cooling radius (R_{cool}).

[b]Accreted mass onto the BH is calculated assuming 10% BH efficiency.

4.2. GALEX Data

Galaxy Evolution Explorer is an Ultraviolet (UV) space telescope, calibration and data products used are presented in Morrissey et. al. (2006). GALEX has a circular field of view of 1.25° and produced a far-UV (FUV) and near-UV (NUV) image simultaneously. The effective wavelengths of FUV and NUV broadband filters are 1540 $\mathring{A}$ and 2320 $\mathring{A}$ respectively. The GALEX data used in this paper are from the GALEX public archives and the public GI database. The magnitude zero point used for FUV and NUV is $m_{FUV} = 18.82$ and $m_{NUV} = 20.08$. First the intrinsic image background was subtracted, then we used Interface Descriptive Language (IDL) routines to derive apparent magnitudes m_{FUV} and m_{NUV} in various aperture radii, for the purpose of discussion in this paper we have used magnitudes and luminosities within the R_e. The integrated apparent magnitudes are then converted into flux using

$$F_{UV} = F_{\circ} 10^{-0.4(m_{UV})} \tag{4}$$

with $F_{\circ,NUV} = 9.289 \times 10^{-9}$ ergs $s^{-1}cm^{-1}$, and with $F_{\circ,FUV} = 2.965 \times 10^{-8}$ ergs $s^{-1}cm^{-1}$, then using

$$L_{UV} = 4\pi F_{UV} D_l^2 \tag{5}$$

L_{FUV} and L_{NUV} were derived. Here D_l is the luminosity distance, calculated based on our cosmology.

4.3. 2MASS Data

In addition to the GALEX data we used Near-Infrared observations done by Two Micron All Sky Survey. We used the K_s (K) band with effective wavelength of 21590 $\mathring{A}$, which is believed to be a good tracer of the old populations of stars. Since gEs are believed to be very old we can be certain that we are observing the entire stellar population of a given galaxy.

The 2MASS data used in this paper were extracted from the 2MASS All Sky Point Source Catalogue (PSC) which is publicly available through NASA/IPAC Extragalactic Database. After the background subtraction, we used IRAF→STSDAS→Analysis→Isophote→ Ellipse package to construct a model of a series of isophotes. This routine allows for masking out pixels therefore unwanted, corrupted and pixels representing foreign sources are disregarded. Ellipse also yields an integrated aperture apparent magnitude, which we found useful in deriving the K-band luminosity using

$$F_K = F_\circ 10^{-0.4(m_K)} \tag{6}$$

with $F_\circ = 4.23 \times 10^{-11}$ ergs $s^{-1}cm^{-1}$ (Cohen et al. 2003), then using

$$L_K = 4\pi F_K D_l^2 \tag{7}$$

Here D_l is the luminosity distance, calculated based on out cosmology. Again, for the purpose of discussion and comparison to the UV data, magnitudes and luminosities were evaluated at R_e. However the total absolute magnitude and K-bad luminosity of the targets were also evaluated at the radii at which the galaxy light approached the background.

The structural parameter, R_e was determined using GALFIT (Peng et al. 2002), which is a publicly available 2D surface brightness profile fitting routine. Effective radius is the radius at which half the light of the galaxy is enclosed. One of the advantages of this program is that it fits a 2 dimensional surface profile models such as Sersic, Nuker, etc. to the image, rather than the 1 dimensional fit to the surface brightness measurements. In a way this method is more reliable in determining the physical properties of the sample. For objects with poor Sersic fits (i.e. GALFIT did not converge, or the presence of a near point source confused GALFIT), we adopted effective radii from the literature, see table 1 for details.

4.4. NVSS Data

The NRAO VLA Sky Survey (NVSS) is a 1.4 GHz continuum survey covering the entire sky north of -40°declination. It uses the Very Large Array, a radio observatory, in its D and DnC configurations between 1993 and 1996(Condon et al. 1998). The data is publicly available at the NVSS website. Almost all of our targets were observed by this survey with the exception of NGC4325 for which no source is detected. The 20 cm radio flux for the targets were retrieved from the NVSS data base. The flux was measured for those targets which did not have a measured flux in the NVSS data base.

Table 3. UV, IR, and 20 cm Radio Properties of the Sample

Target	M_K	(NUV-K)[a]	(FUV-K)[a]	$L_K(R_e)$[b] (10^{42} erg s^{-1})	$L_{NUV}(R_e)$[b] (10^{42} erg s^{-1})	$L_{NUV}(R_e)$[b] (10^{42} erg s^{-1})	$L_{Radio,1400}$[b c] (10^{38} erg s^{-1})
NGC315	-26.52	9.30	10.12	188.00	2.670	0.262	3.54
NGC507	-25.94	9.29	10.47	48.50	0.698	0.049	0.1595*
NGC777	-26.15	9.05	9.64	148.00	2.650	0.321	218.985
NGC1316	-26.24	8.97	10.58	127.00	2.460	0.116	8.404
NGC1600	-26.33	9.10	8.48	174.00	0.622	5.310	0.4629
NGC3077	-18.29	6.03	6.75	0.13	0.041	0.004	1.9984
NGC3608	-23.16	8.31	9.70	16.50	0.587	0.034	6.8E-4*
NGC4325	-24.99	8.55	9.89	65.40	1.850	0.112	...
NGC4374	-24.53	8.72	9.94	48.00	1.190	0.080	0.935*
NGC4552	-22.03	8.61	9.16	2.96	0.080	0.010	0.2992
NGC5044	-25.25	8.90	9.42	50.20	1.030	0.133	14.702
NGC5252	-25.46	8.03	8.42	95.60	4.380	0.637	9.468
NGC5253[d]	-20.22	3.68	4.18	1.02	2.580	0.340	8.019
NGC5813	-24.57	8.86	9.76	71.90	1.540	1.400	49.57
NGC5846	-24.95	9.00	9.53	40.00	0.753	0.096	0.0361
NGC6269	-26.42	9.59	10.32	72.90	0.798	0.085	2.053
NGC7626	-25.49	9.15	9.94	59.30	0.963	0.097	616.257
UGC408	-24.81	9.57	9.59	13.90	0.155	0.032	87.951*

[a]The colors are measured at (R_e), refer to Table 1.

[b]The uncertainty in these measurements will be determined in the near future, due to time constraints they are not included in this paper.

[c]The radio luminosities are measured at 1400MHz and include the radio point source and in some cases the extended lobes.

[d]NGC 5253 is classified as a star burst galaxy in the literature, hence the relatively blue color.

Note. — The targets marked with '*' represent the few objects for which radio flux was not available through the NVSS data base and therefore it was measured.

5. Results and Discussions

The light observed from a star forming region is mainly due to hot, massive stars such as O and B stars. At temperatures exceeding 30000 K, these stars emit most of their light at Ultraviolet wavelengths. Ultraviolet emission is highly sensitive to extinction. This is the reason star formation can not be readily observed, because star forming regions are surrounded by the excess gas and dust that were not consumed in the star forming process, and the star light is scattered. There has been numerous procedure proposed for estimating star formation rates. Recently Salim et al. (2007) suggested a relationship for estimating star formation rates (SFR) in the local universe using UV luminosity:

$$SFR(M_{\odot}yr^{-1}) = 1.4 \times 10^{-28} L_{\nu}(ergs^{-1}s^{-1}Hz^{-1}) \tag{8}$$

We derived L_{FUV} and L_{NUV} from the GALEX data, normalized to the frequency at their respective wavelengths and used equation (6) to derive SFR. We have SFRs at various aperture radii with respect to the cooling radius. For the purpose of discussion the SFRs presented in this paper are at 30% of R_{cool}. This aperture seemed to be a very acceptable size based on visual inspection of all object, at which the UV light was completely encompassed.

Table 4. Star Formation Rates of the Sample

Target	SFR_{NUV} ($M_\odot\ yr^{-1}$)	SFR_{FUV} ($M_\odot\ yr^{-1}$)
NGC315	0.0980	0.0640
NGC507	0.8950	0.5670
NGC777	0.3050	0.1790
NGC1316	0.2560	0.0930
NGC1600	0.1750	0.1370
NGC3077	0.0010	0.0008
NGC3608	0.0390	0.0130
NGC4325	0.4710	0.1920
NGC4374	0.0780	0.1310
NGC4552	0.0050	0.0040
NGC5044	1.3230	0.9450
NGC5252	0.3030	0.2540
NGC5253	0.1020	0.0880
NGC5813	0.2380	0.2160
NGC5846	0.1440	0.1640
NGC6269	0.2170	0.1450
NGC7626	0.1590	0.0670
UGC408	0.1970	0.2750

Note. — As mentioned in the text, star formation rates have been measured with in $0.3R_{cool}$.

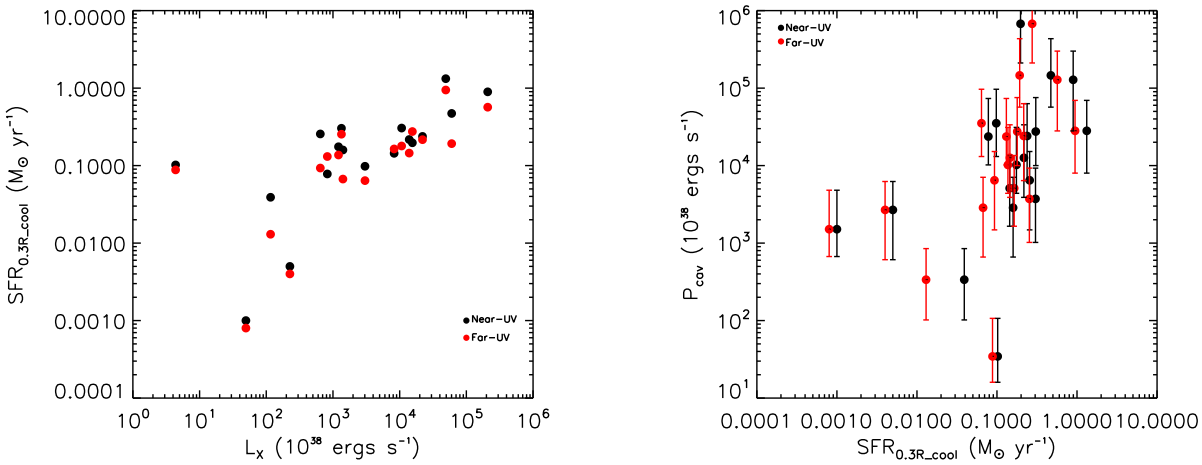

Fig. 1.— X-ray luminosity plotted against star formation rate (left) and AGN jet power plotted against star formation rates (right).

Shown in Fig. 1 is the X-ray luminosity and AGN jet power versus the SFR. It is observed a very strong trend in L_X vs. SFR mainly, objects with higher cooling rates, higher SFR is observed. This is inevitable in the sense that if there is more gas cooling and condensing onto the galaxy there will be more gas readily available to clump and form stars. the AGN was assumed to be the heating mechanism. An anti-corelation was expected in P_{cav} vs. SFR. The expected relation would have implied less star formation in targets with higher AGN outburst. However this is not the case as seen in Fig. 1, this suggest there should be other mechanisms at work in heating the ICM and that the AGN alone is not sufficient to limit star formation.

Star formation rates and UV-K colors, are plotted as a function of ratio of jet power (heating mechanism) to X-ray luminosity (cooling mechanism) in fig. 2. If this ratio is smaller than 1, then the galactic medium is cooling more than it is being heated and if the ratio is greater than 1, the medium is being heated more than it is being cooled. The higher (UV-K) index signified a redder galaxy and a lower (UV-K) index represents bluer galaxies.

NGC5253 and NGC3077 are significantly blue relative to the majority of our sample. Bluer objects would in theory signify more star formation, the average star formation in NUV and FUV for the objects are 0.095 and 0.0009 respectively. The SFRs for these two galaxies are not very large in comparison to the rest of our sample. Active galactic nuclei emit some light in the UV region of the electromagnetic spectrum. Therefore it is posited that NGC3077 and NGC5253 blue colors may be caused by the fact that the AGN in these galaxies is very luminous and the UV light emitted by the AGN makes this galaxy appear very blue.

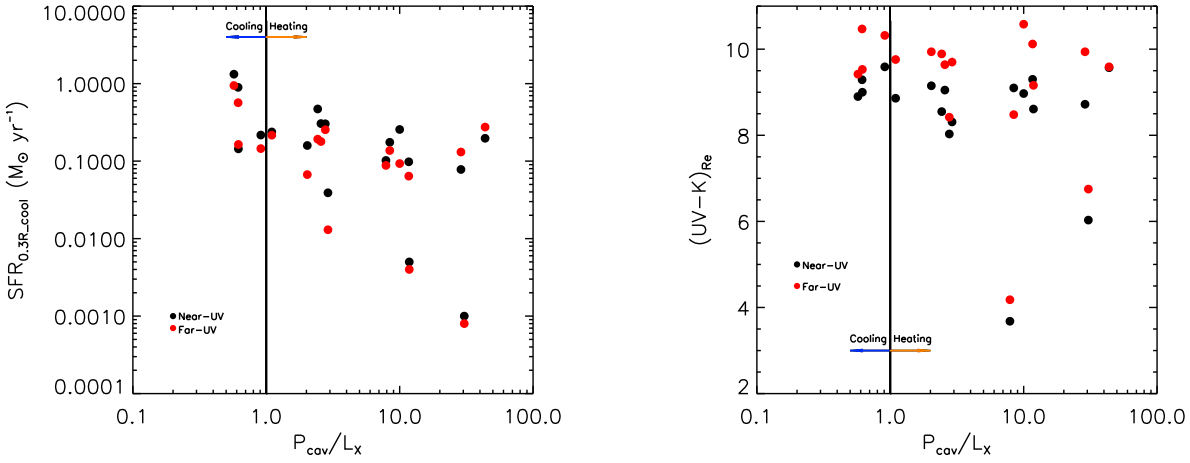

Fig. 2.— SFR and UV-K color against ratio of P_{cav}/L_X. The cooling and heating sides are marked. Decreasing color value signifies bluer objects and increasing color value signifies redder objects.

Figure 3 shows the color-magnitude diagram for the sample. It is very clearly observed that our targets form a red sequence, as they are very old galaxies in the local universe. The two outliers are again NGC3077 and NGC5253. It has not yet been determined if these two objects are part of the extended red sequence of they are either in the green belt or the blue could. The blue color of these two galaxies would suggest that they are not part of the red sequence, however the very low SFR leads to the conclusion that they are an extension of the red sequence of galaxies.

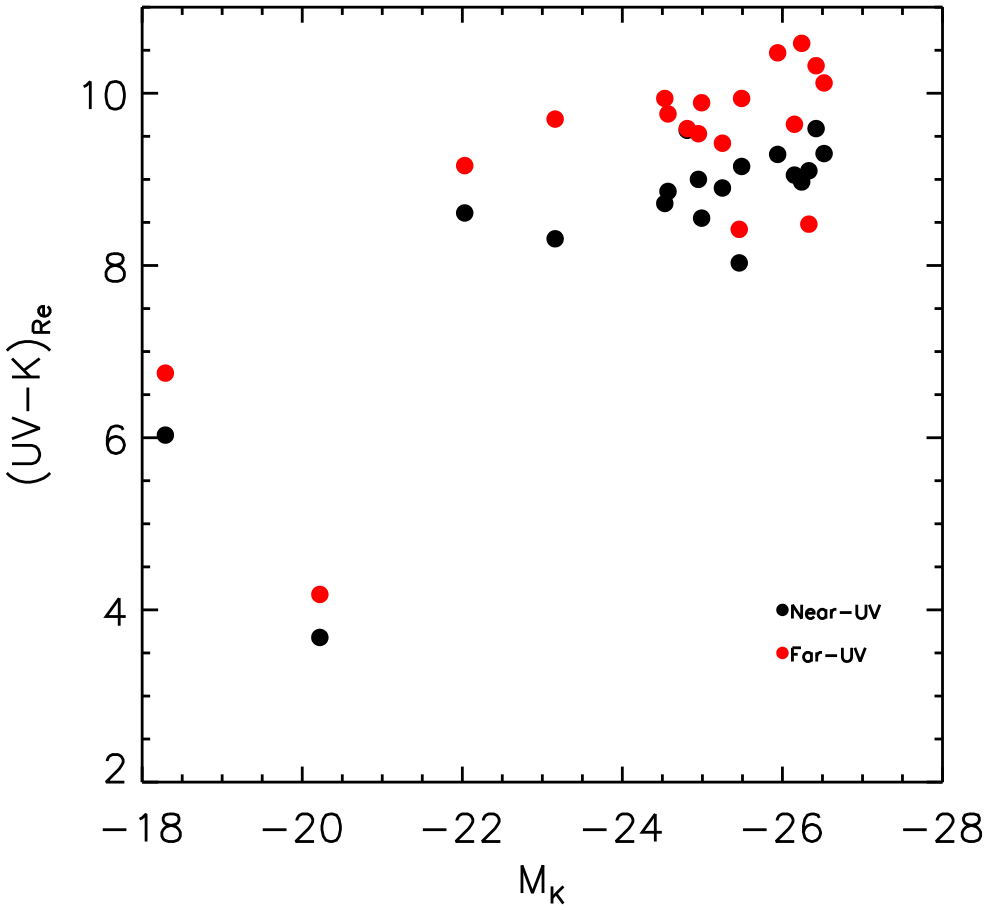

Fig. 3.— The UV-K color vs. absolute K-band magnitude.

In Fig. 4 cavity power is plotted vs. nuclear radio synchrotron power at 20 cm. It is assumed that the cavities have been created by the mechanical work done by the relativistic jets originating from the BH. The large ratio of these quantities shows that the energy released by the extragalactic radio sources is largely mechanical, and thus they are efficient at heating the surrounding plasma.

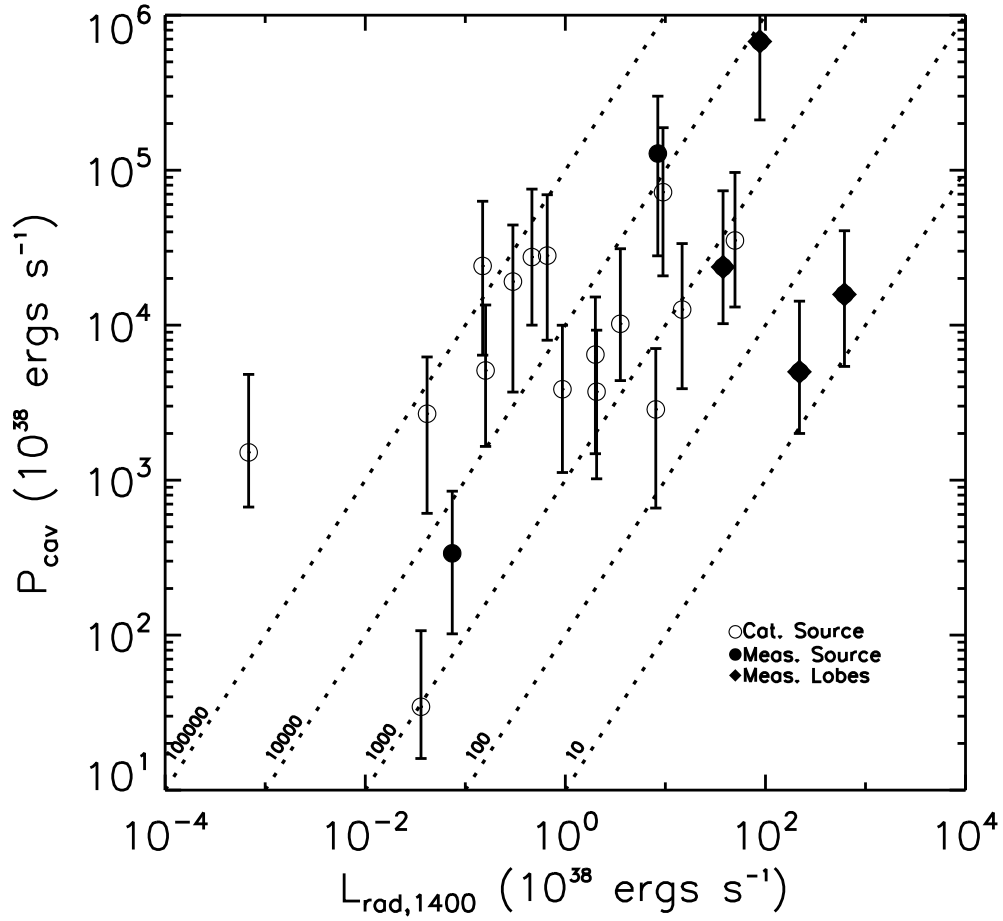

Fig. 4.— Mechanical power vs. 1400MHz nuclear radio source luminosity.

The Magorrian relation is one which describes the connection between the size of the BH to the size of the galaxy. $M_{BH}/M_{bulge} = (1.4 \pm 0.4) \times 10^{-3}$ (Häring & Rix 2004), means that the mass of the bulge of a galaxy is $\sim$ 700 times larger the mass of the BH it harbors. In a sense this relation can be extended to explain the growth rate of the BH and the growth rate of the host galaxy. Growth rate of the BH is understood to be the amount of gas/dust it accretes in a unit time, in our case $\dot{M}_{BH}$ in $M_\odot\ yr^{-1}$, and the growth of the galaxy is assumed to be the amount of stars that are formed from the in-falling gas as the result of the

cooling flows, in our case SFR in in $M_{\odot}\ yr^{-1}$. In § 4.1 the derivation of $\dot{M}_{BH}$ is discussed. Figure 5 shows the growth rate of the BH vs. the growth rate of the galaxy. Over plotted are diagonal lines representing the Magorrian relation at BH energy conversion efficiencies ϵ = 0.1(static BH) - 0.4(spinning BH).

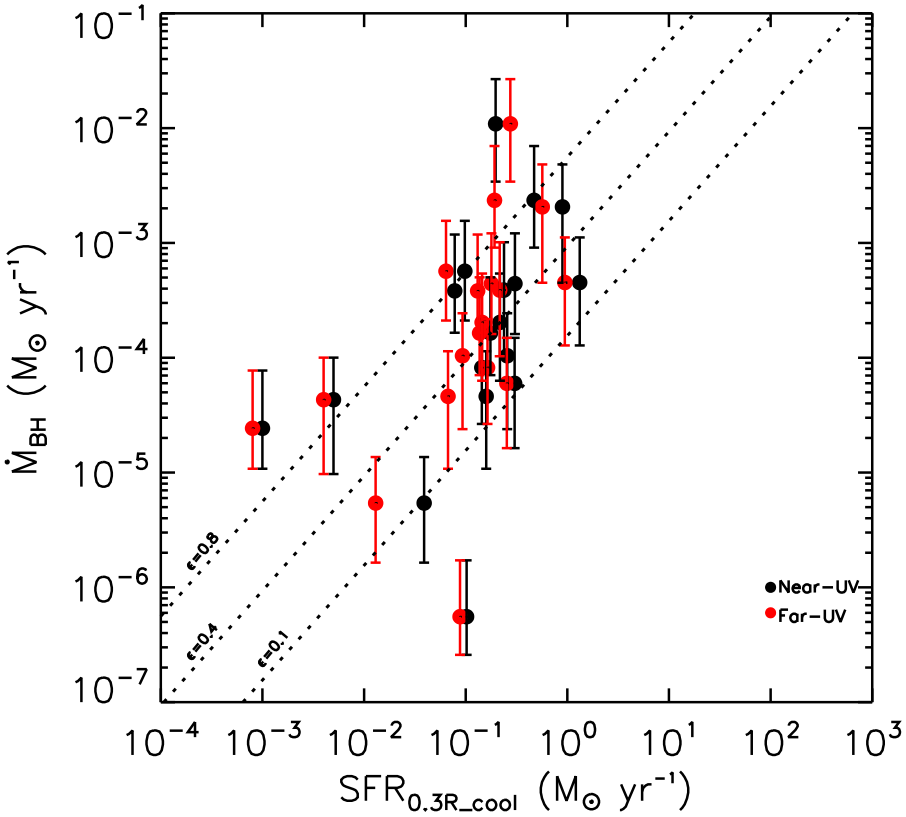

Fig. 5.— The growth of the BH is plotted against the growth of the bulge, the Magorrian relation, $\dot{M}_{BH} = 1.4 \times 10^{-3}$ SFR, has been plotted in dotted lines at various BH energy conversion efficiencies $\epsilon = 0.1, 0.4, 0.8$.

Most of our targets fall within the acceptable limits of the BH conversion efficiency. However there are some outliers which display BH conversion efficiency of $\epsilon = 0.8$ and higher. These efficiencies are not physical, in other words a BH can not be this efficient in converting

the rest mass energy of the in-falling matter into outburst energy. It is posited that the BH-bulge growth happens in step wise manner. At one given time the BH goes through a feeding frenzy and growing and at another time the galaxy goes through a star burst. Hence the BH-bulge growth does not happen simultaneously. Therefore the Magorrian relation is a time average of the BH-bulge growth.

6. Conclusions and Future Work

We have presented star formation rate for 18 gEs. The effect of the heating mechanism (AGN feedback), and cooling by the ICM (cooling flows) on the star formation is investigated. In order to have ideal conditions for star formation the cooling flow mechanism has be very efficient. We used Ultraviolet observations (GALEX) and equation (6) to derive SFR for our samples, the average SFR_{NUV} is 0.2781 and SFR_{FUV} is 0.1964 $M_{\odot}yr^{-1}$. We also used Near-Infrared observations (2MASS) to have a better understanding of the old stellar of population of the target galaxies. We observed that with higher cooling rates, higher X-ray luminosity, there is evidence of higher SFR in the galaxies. There is also a trend observed in AGN power output and SFR. We expected to see lower SFR in galaxies with higher AGN power, however this is not the case. This can be explained by positing that the BH is accreting hot gas at the center of the galaxy as oppose to cold gas, this process is named Bondi accretion.

We observe higher SFR in galaxies with ratio of AGN power to cooling luminosity smaller than 1 and lower SFR in galaxies with ratio of AGN power to cooling luminosity greater 1. This finding exhibits that if cooling flow is more efficient than the AGN feedback more gas would be available to form stars in the galaxy. The heating to cooling ratio is compared against (UV-K) color, no suggestive trend is observed, however we do notice NGC3077 and NHC5253 having relatively blue colors, yet are currently being heated. These two galaxies have very low SFR, the average star formation in NUV and FUV for the objects are 0.095 and 0.0009 respectively, which are low relative to the rest of the sample. The blue color of these galaxies could be explained by a very luminous AGN. The color-magnitude diagram for our sample shows very clearly a red sequence, which was expected given that our sample consists of gEs in later stages of their evolution. Again, NGC3077 and NGC5253 have very blue colors. This could suggest that these two galaxies maybe part of the blue cloud or the

green valley on the color-magnitude diagram. Or they could be the extension of the red sequence.

It is observed that the radio synchrotron power at 20 cm (1400MHz) is not very efficient in doing mechanical work, however the presence of cavities in this system suggests that the AGN is very efficient in heating the surrounding gas in the ICM. This suggests that the BH is out putting the majority of its energy in mechanical work.

The Magorrian relation explaining the relation between the growth of the BH and the bulge of the galaxy, $\dot{M}_{BH} = 1.4 \times 10^{-3}$ SFR, was adopted (Häring & Rix 2004). Applying this relation to our sample, it is observed that the majority of our targets obey the prediction of this relation. However there are some objects which exceed or are inferior to this relation. We posit that the growth of galaxy system, BH and bulge happen in step wise manner, the BH would accrete for a certain amount of time and the galaxy will go through a star burst at another given time. The Magorrian relation is simply the time average of this step wise process.

It would be ideal to derive SFR using $H\alpha$ and Far-Infrared data and compare to the quantities derived using UV data. This would provide a concrete and incontestable SFR for our sample. In order to be able to claim that the relativistic jets from the BH are not fully responsible for creating the cavities, the bolometric radio luminosity is needed to be compared to the mechanical energy that created the cavities. Our data needs to be corrected for galactic extinction and k and evolutionary corrections. Lastly, the uncertainty in SFR and UV and K luminosities has to be determined.

7. Acknowledgments

I would like to thank C. Peng for creating GALFIT and making it publicly available. GALEX, 2MASS, and NRAO teams for making their archival data publicly available, Dr. P. Nulsen for providing me with the sample, jet power and cooling luminosity calculations, and C. Kirkpatrick for helpful discussions. I am grateful to Dr. B. McNamara for giving me this opportunity and for his invaluable insight, guidance and support thus far.

REFERENCES

Barbon, B., Benacchio, L., Capaccioli, M., & Rampazzo, R., 1984, A&A, 137:166-176

Bîrzan, L., Rafferty, D. A., McNamara, B. R., Wise, M. W., & Nulsen, P. E. J. 2004, ApJ, 607, 800

Cohen, M., Wheaton, Wm. A., & Megeath, S. T., 2003

Condon, J. J., Cotton, W. D., Greisen, E. W., Yin, Q. F., Perley, R. A., Taylor, G. B., & Broderick, J. J. 1998, AJ, 115, 1693

de Zeeuw, P. T., et al. 2002, MNRAS, 329, 513

Evans II, N. J., 1999, ARA&A, 37:311-62

Fabian, A. C., 1994, ARA&A32:277-318

Häring, N., & Rix, H.-W. 2004, ApJ, 604, L89

Knapp, G. R., 1998, (astro-ph/9808266)

Lin YT, Mohr JJ, Stanford SA. 2003. AJ, 591:749-763

Marlowe, A. T., Meurer, G. R., & Heckman, T. M., 1999, AJ, 522:183-198

McNamara, B. R., & Nulsen, P. E. J. 2007, ARA&A, 45, 117

Morrissey, P., Conrow, T., Barlow, T. A., Small, T., Seibert, M., Wyder, T. K., Budavari, T., Arnouts, S., Friedman, P. G., Forster, K., Martin, D. C., Neff, S. G., Schiminovich, D., Bianchi, L., Donas, J., Heckman, T. M., Lee, Y-W., Madore, B. F., Milliard, B., Rich, R. M., Szalay, A. S., Welsh, Y., & Yi, S. K. 2007, ApJS, GALEX Issue

Peng, C. Y., Ho, L. C., Impey, C. D., & Rix, H., 2002, AJ, 124:266-293

Rafferty, D. A., McNamara, B. R., Nulsen, P. E. J., & Wise, M. W., 2006, AJ, accepted

Salim, S., Rich, R. M., Charlot, S., Brinchmann, J., Johnson, B. D., Schiminovich, D., Seibert, M., Mallery, R., Heckman, T. M., Forster, K., Friedman, P. G., Martin, D. C., Morrissey, P., Neff, S. G., Small, T., Wyder, T. K., Bianchi, L., Donas, J., Lee Y-W. Madore, B. F., Milliard, B., Szalay, A. S., Welsh, B. Y., & Yi, S. K., 2007, ApJS, GALEX Issue

Sarazin, C. L., 1988, Cambridge University Press

Soltan, A., 1982, Royal Astronomical Society, 200:115-122